We are IntechOpen,
the world's leading publisher of Open Access books
Built by scientists, for scientists

6,900
Open access books available

186,000
International authors and editors

200M
Downloads

Our authors are among the

154
Countries delivered to

TOP 1%
most cited scientists

12.2%
Contributors from top 500 universities

CLARIVATE ANALYTICS
BOOK CITATION INDEX
INDEXED

WEB OF SCIENCE™

Selection of our books indexed in the Book Citation Index
in Web of Science™ Core Collection (BKCI)

Interested in publishing with us?
Contact book.department@intechopen.com

Numbers displayed above are based on latest data collected.
For more information visit www.intechopen.com

Chapter

Development of a Corona Discharge Ionizer Utilizing High-Voltage AC Power Supply Driven by PWM Inverter for Highly Efficient Electrostatic Elimination

Katsuyuki Takahashi, Koichi Takaki, Isao Hiyoshi,
Yosuke Enomoto, Shinichi Yamaguchi and Hidemi Nagata

Abstract

The corona discharge ionizer has been widely used to eliminate electrostatic charges on insulators in a variety of manufacturing industries for the prevention of electrostatic discharge (ESD) problems. High-speed electrostatic elimination is conventionally required for ionizer performance. Because of the high sensitivity of recent electronic devices to ESD damage, an extremely low-offset voltage (ion balance) is required for the performance of electrostatic eliminators. Long-term performance stability is required to maintain the quality of the products, but the short cleaning interval of the unit increases the operating cost. The efficiency is also affected by the waveform of the applied voltage. The optimization of the applied voltage is an important factor in achieving long-term performance stability. In this study, an intermittent pulse voltage AC power supply was developed to achieve a highly efficient electrostatic elimination with long-term stability high-speed electrostatic elimination and an excellent ion balance.

Keywords: electrostatic, ionizer, corona discharge, ion balance, high voltage

1. Introduction

Elimination of electrostatic charges on insulators for the prevention of electrostatic discharge (ESD) problems in manufacturing industries such as semiconductor and electric device is very important for the enhancement of productivity and reliability [1–5]. The simplest and the most important method to prevent ESD is eliminating charges by keeping conductive materials connected to the ground. In work spaces, wearing anti-ESD wrist straps and conductive clothes and shoes and keeping conductivity of tables and floors high are required for ESD control. In the case of insulators, charges are not removed by connecting them to the ground. Therefore, generally, the charges accumulated on insulators are decayed by decreasing the

surface resistance by increasing humidity. Although these methods are effective for the prevention of ESD problems, they are restricted by environment, materials, and conditions of objects. When these methods are unavailable, the methods to forcibly eliminate the charges by neutralizing using ions are required.

The corona discharge ionizer has been widely used for elimination of electrostatic charges because of its good operability. **Figure 1** shows schematic illustration of elimination of electrostatic charge accumulated on an insulator using an ionizer. The corona discharges are produced at high-voltage electrodes in the ionizer, which enable the production of positive and negative ions such as H_3O^+, CO_3^-, NO_3^-, and their cluster ions [6–9, 10]. The ions produced by the corona discharges are transported by the electric field or blown air to insulators, and the charges on insulators are neutralized by the ions. The time required for the electrostatic elimination depends on the amount of ions transported to the insulators. For the ionizer performance, not only the short electrostatic elimination time but also the good ion balance (a low-offset voltage), the balance between the amounts of ions of both polarities (**Figure 2**), is required
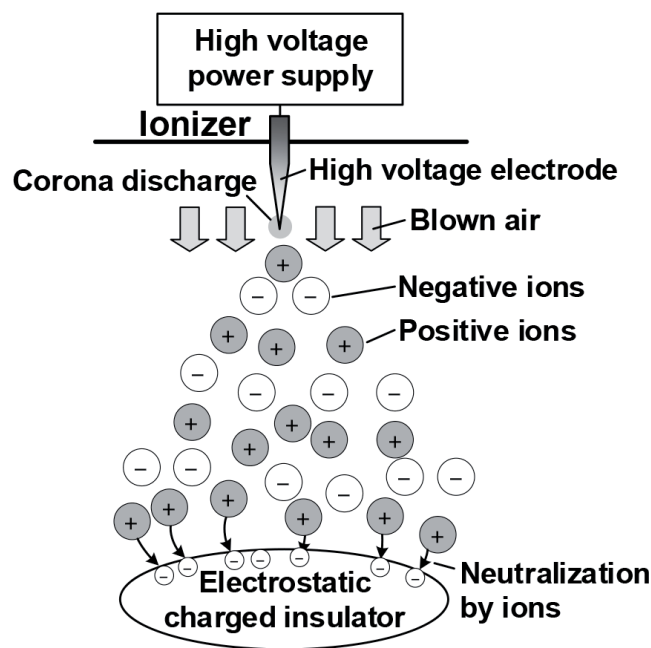

Figure 1.
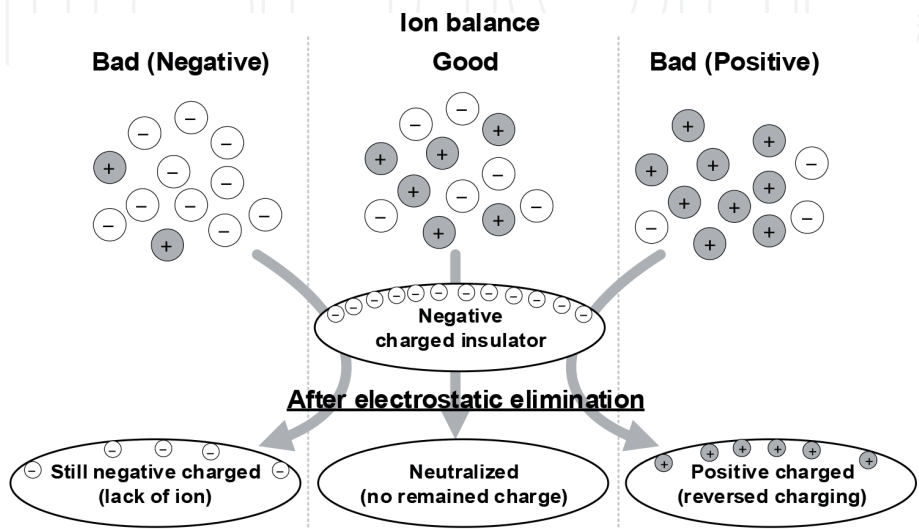*Schematic illustration of elimination of electrostatic charge accumulated on an insulator using an ionizer.*

Figure 2.
Relationships between ion balance and electrostatic charges on insulator after electrostatic elimination.

	DC	Commercialized frequency AC (50/60 Hz)	Rectangular AC (< 100 Hz)*	Intermittent bipolar pulse (several hundred Hz)	High frequency AC (several tens kHz)
Electrostatic elmination without blown air	Excellent	Average	Good	Below Average	Inferior
Ion balance unevenness in deionzing space	Inferior	Average	Below Average	Good	Excellent
Ion balance fluctuation	Average	Inferior	Inferior	Good	Excellent
Performance stability	Inferior	Average	Average	Excellent	Inferior
Size and weight	Average	Inferior	Below Average	Good	Excellent

*Pulsed AC type ionizer and pulsed DC type ionzer

Table 1.
Characteristics of typical corona discharge ionizers for the various types of voltage supplies.

[11–14]. The bad ion balance causes ESD problem on the latest electronic devices, which have high sensitivity to ESD damage. For example, the ion balance is limited less than 25–100 V in the manufacturing process of electric devices, and only several volts in the process of hard disc heads have a very high sensitivity for ESD [15–18].

The polarity of the ions produced by the corona discharges is the same as the polarity of the applied voltage to the needles [19, 20]. **Table 1** shows the characteristics of the typical corona discharge ionizers for the various types of voltage supplies. The corona discharge ionizers are mainly characterized by the frequency of the applied voltage to the electrodes. There are advantages and disadvantages with each frequency, which require an optimum selection for each situation.

The charge decay time, the time required to eliminate electrostatic charge on a charged object, is significantly affected by the amplitude of applied voltage to the needles, the voltage waveform, and its timing and frequency. Usually, the ions are transported to the charged objects by blown air using a fan or compressed air. When the blown air is limited, the ions must be transported by Coulomb force along the electric field from the needle and by self-diffusion [21]. In this case, DC and low-frequency and commercialized AC are suitable for electrostatic elimination because the polarity change of the electric field is slow and ions are efficiently transported to the object; on the other hand, the fluctuation width of the ion balance becomes large with low-frequency AC [21]. The fluctuation causes ion balance unevenness in the deionizing space [20, 22, 23]. Although a high-frequency AC requires blown air for electrostatic elimination due to its rapid polarity change, the well-mixed positive and negative ions suppress the fluctuation of the ion balance.

Long-term performance stability is required to maintain the quality of the products, but the short cleaning interval of the unit increases the operating cost. The performance of the electrostatic eliminator declines with the deterioration of the high-voltage electrode because of dust attraction and abrasion from the corona discharge. The amount of ions produced by corona increases with discharge current which depends on amplitude of applied voltage and geometry of electrode [24, 25], which decreases the charge decay time. On the other hand, the efficiency of electrostatic elimination decreases with increasing discharge current that does not contribute to eliminating electrostatic charge, which causes electrode deterioration. The efficiency is significantly affected by the waveform of the applied voltage. DC-type ionizers have two polarity electrodes. Since the abrasion of the electrode depends

on the polarity, the balance of the positive and negative ions collapses. In the high-frequency AC ionizers, the ions are easily lost by the ion-ion recombination reaction, and the efficiency for ion transport to the charged object is very low. The optimization of the applied voltage is an important factor in achieving long-term performance stability.

In this study, an intermittent pulse voltage AC power supply with a small and lightweight transformer was developed for highly efficient electrostatic elimination. A corona ionizer driven by a power supply offers long-term performance stability in low-offset voltage. The high stability enables the installation of an electrostatic eliminator in the manufacturing processes of high electrostatic-sensitive devices required for extremely low-offset voltage. In this chapter, the specifications of the power supply and the electrostatic eliminator are outlined with quantitative data.

2. Bipolar pulse voltage power supply driven by PWM converter

Figure 3 shows a schematic diagram of the bipolar pulse voltage power supply driven by a full-bridge PWM converter [26]. The primary current of the transformer is controlled by a full-bridge converter circuit consisting of four MOSFETs with a DC voltage supply (V_{DD}). The value of V_{DD} depends on the turn ratio of the transformer and is 24 V for this example. The MOSFETs are driven by PWM input signals (Q_1–Q_4) generated by a microcomputer through the FET driver circuits. The ON signal and PWM signal are outputted to Q_1 and Q_4, respectively, in a positive phase; the ON signal and PWM signal are outputted to Q_3 and Q_2, respectively, in a negative phase. **Figure 4a** shows the relationship between the output voltage and the control signals. The amplitude of the pulse voltage is adjusted by the duty ratio of the PWM signals at the rising edge of the pulse. The PWM signals at the falling edge of the pulse suppress the ringing induced by the resonance, which contributes to generating a pulse shape close to an ideal condition. **Figure 5** shows the typical waveform of the output voltage controlled by the PWM signals. The amplitude, interval, and generation timing of the pulses can be arbitrarily set according to the PWM signals as shown in **Figure 4b**, which realizes the generation of not only intermitted pulse voltage but also AC sinewave voltage.

The frequency and pulse width of the output voltage are determined by the characteristics of the transformer such as the material and the cross section of the core and the number of turns of the coil. Since the characteristics of the
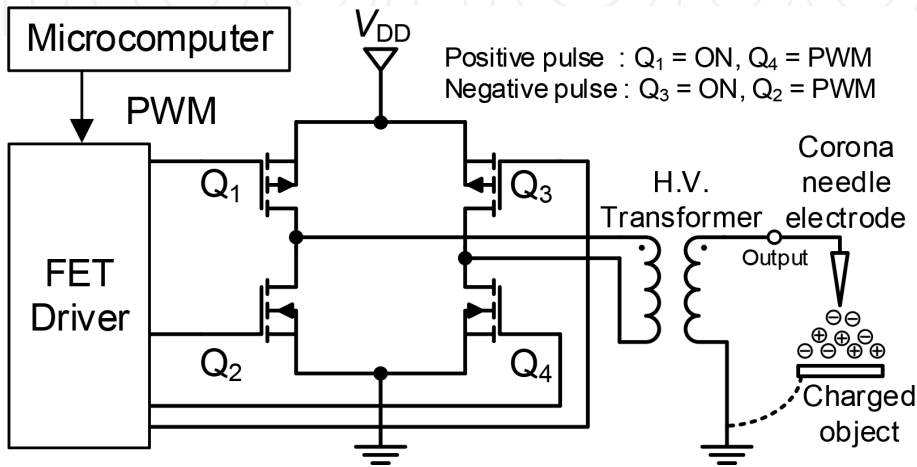

Figure 3.
Schematic diagram of the bipolar pulse voltage power supply driven by a full-bridge PWM converter [26].
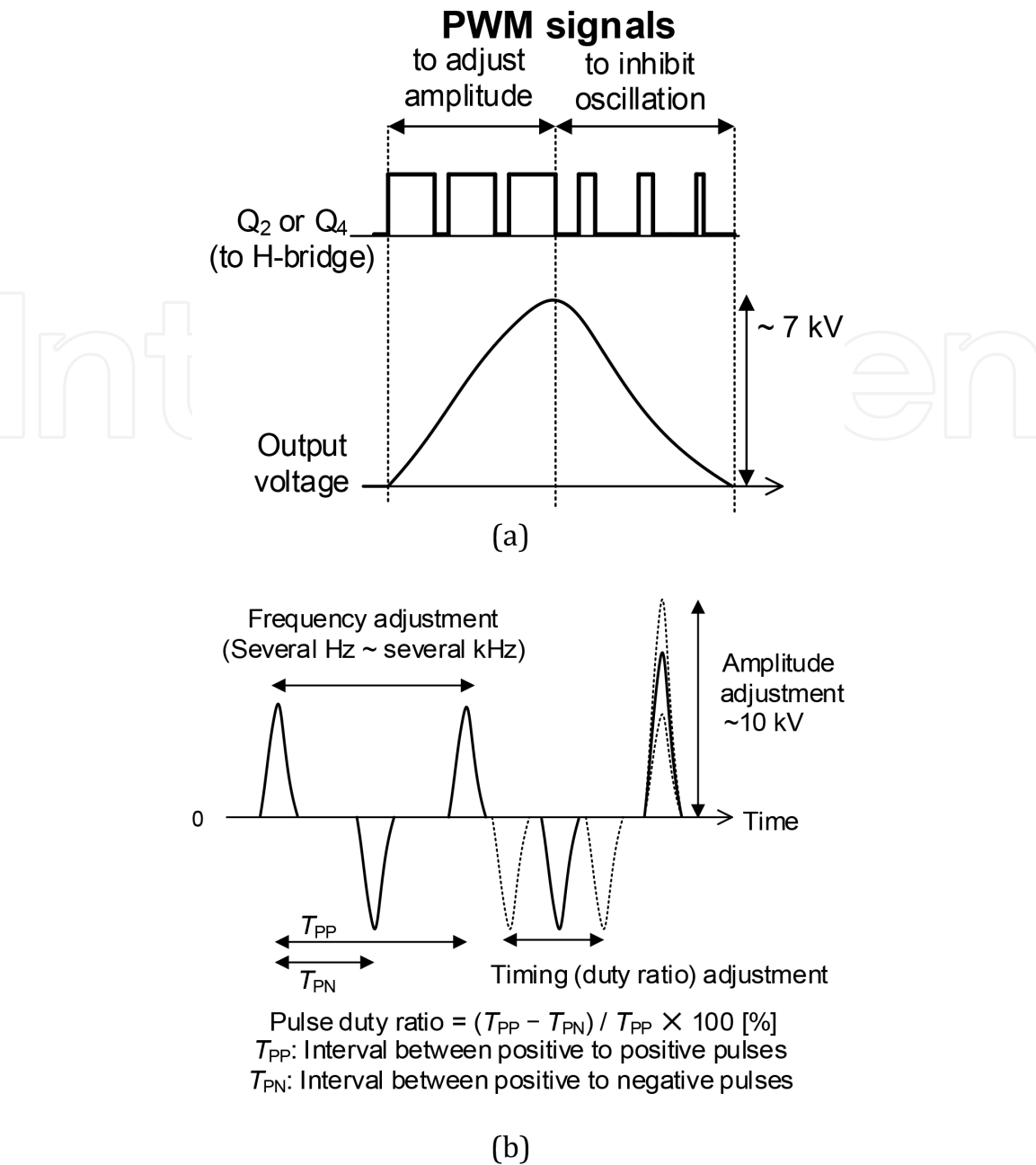
PWM signals

to adjust amplitude   to inhibit oscillation

Q_2 or Q_4
(to H-bridge)

~ 7 kV

Output voltage

(a)

Frequency adjustment
(Several Hz ~ several kHz)

Amplitude adjustment
~10 kV

0

Time

T_{PP}

T_{PN}

Timing (duty ratio) adjustment

Pulse duty ratio = $(T_{PP} - T_{PN}) / T_{PP} \times 100$ [%]
T_{PP}: Interval between positive to positive pulses
T_{PN}: Interval between positive to negative pulses

(b)

Figure 4.
*Schematic diagram of PWM control [26]. (a) Relationship between the output voltage and the control signals,
(b) output voltage.*

Pulse

Ringing

Controlled
Uncontrolled

Figure 5.
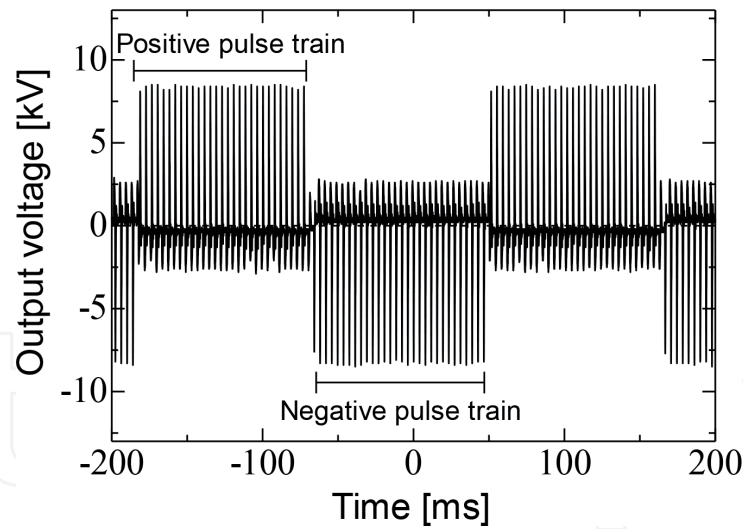*Typical waveform of output voltage [26].*

Figure 6.
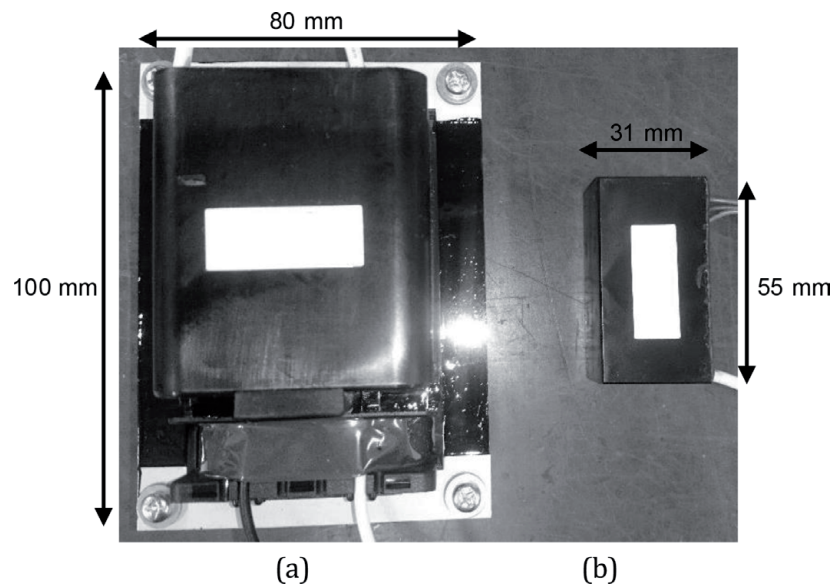*Typical waveform of continuously generated pulse train [26].*

Figure 7.
Photograph of two transformers [27]. (a) Commercial frequency, (b) bipolar intermittent pulse.

electrostatic eliminator depend on the frequency as mentioned above, the various types of transformers are prepared for various applications to generate the optimized frequency. Generally, the magnetic flux inside the core required to magnetically couple the primary and secondary windings increases with decreasing the frequency, which increases the size and weight of the transformer. To generate the low-frequency voltage with a small and lightweight transformer, the same polarity pulses are continuously generated in a phase as a pulse train by the PWM converter, and the polarity is switched with a period, as shown in **Figure 6**. The apparent frequency decreases with increasing number of pulses in the period. The unipolar pulse train can continuously generate unipolar ions in a phase and transport them to the charged object by the electric field and self-diffusion, which contributes to improving the electrostatic elimination speed without blown air, as described later.

The bipolar pulse voltage power supply driven by a full-bridge PWM converter provides a certain degree of freedom in generating the pulse voltages. **Figure 7** shows a photograph of a transformer designed for commercial frequency (50 or 60 Hz) and a transformer designed for the bipolar intermittent pulse with a frequency of 250 Hz [27]. The turn ratios are 70 and 360. The cores are both made

using a silicon steel sheet. Although the transformer designed for the bipolar inter-
mittent pulse is over 10 times smaller and lighter than the transformer designed for
commercial frequency, the performance for electrostatic elimination is almost the
same in many situations with the optimum voltage waveforms controlled by PWM
control. The optimization of voltage waveforms in various applications realizes a
design of small and lightweight systems and a long-term performance stability.

3. Evaluation method of electrostatic elimination performance of ionizer

The charge plate monitor (CPM) is usually used for evaluation of electrostatic
elimination performance of ionizer. CPM consists of a metal plate with a plate-to-
ground capacitance of 20 ± 2 pF [28]. The plate is charge to higher than ±1 kV [28],
and the voltage is reduced by the ionic current caused by ion flow in the plate. The
electrostatic elimination time is defined as time required for decreasing the plate
voltage from ±1 kV to ±100 V. The ionic current flow to the plate is determined by
the temporal change of the plate voltage according to an equation, $i = \mathrm{d}q/\mathrm{d}t = C\,\mathrm{d}v/\mathrm{d}t$.
The ion current measuring device such as CPM is required for a high insulation
resistance, a low capacitance, and a high-voltage charge because the ionic current
into the insulators is on the order of 10^{-9} A [29]. The frequency response of the
CPM is limited by these requirements, which causes an incorrect measurement. For
example, the frequency response of the conventional CPMs is lower than 100 Hz.
Furthermore, the displacement current induced by the high voltage applied to the
corona discharge electrodes interferes with the measurement of the ionic current.

Figure 8 shows a schematic diagram of the ion measuring system developed
for a precise evaluation of the ionizer with a high-frequency component [30].
The system consists of the ion-trapping metal plate, capacitors C_{I1} consisted
of three series capacitors (WIMA, FKP2-33/1000/10, 33 pF) and C_{I2} (KEMET,
PHE448SB4100JR06, 1 nF), and a buffer circuit op-amp A_1 (Texas instruments,
OPA454). The ion-trapping plate voltage (v_I), usually higher than ±1 kV, can be
determined by measuring the voltage across C_{I2} using the buffer circuit as a low volt-
age because the ion-trapping plate voltage (v_I) is divided by C_{I1} and C_{I2}. The buffer
circuit does not interfere with measuring v_I because of its very high input impedance
($10^{13}\Omega$) and low-bias current (1.4 pA). The ratio between v_I and the output voltage of
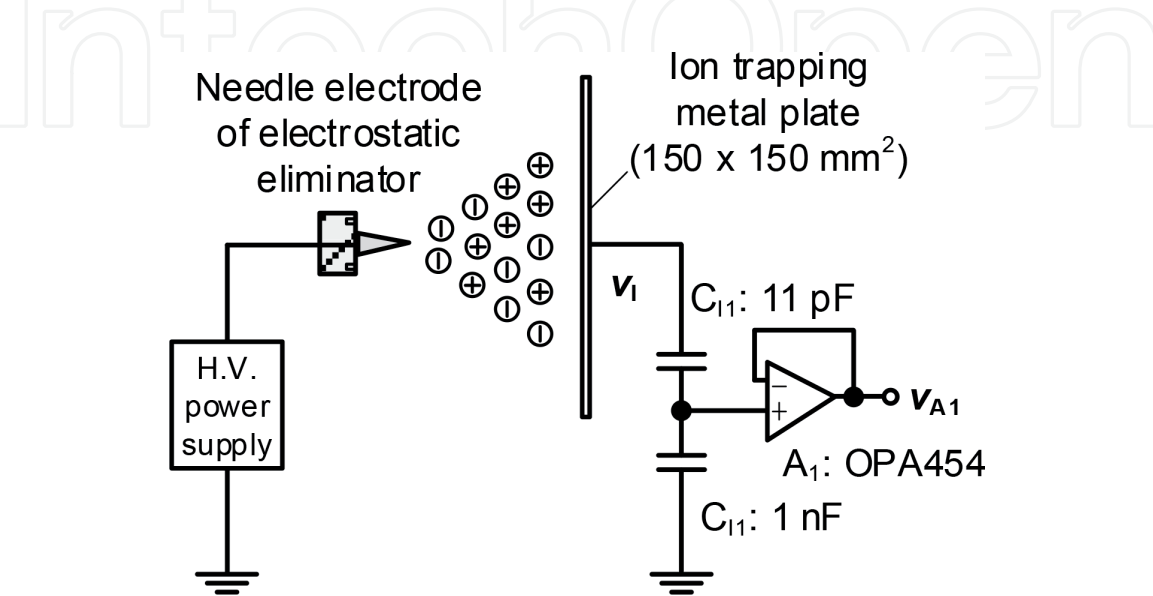the buffer circuit (v_{A1}) is determined by the capacitances of C_{I1} and C_{I2}. The op-amp

Figure 8.
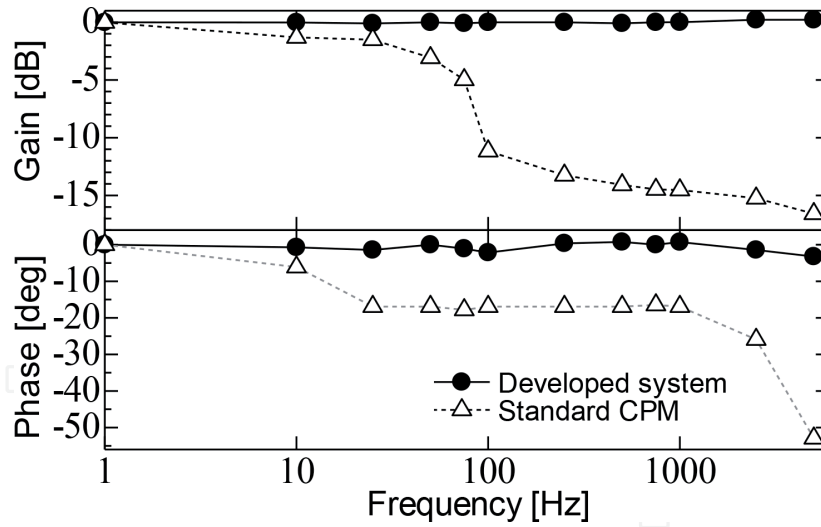*Schematic diagram of the ion measuring system.*

Figure 9.
Bode plots for the developed system and the standard CPM.

allows to apply the input voltage less than ±50 V. Therefore, in the system shown in **Figure 6**, the maximum voltage that can be applied to the plate is 4.25 kV. The total capacitance between the ion-trapping plate and ground is 21.2 pF with the plate area of 150 × 150 mm^2, which is based on a standard established by ESD association [28].

To compare the developed system with a conventional ion evaluation and ion measuring device, a standard CPM (Trek, Model 158) is employed. **Figure 9** shows the bode plots for the developed system and the standard CPM [30]. The gain and phase shift have constant values in the case of the developed system with the frequencies lower than 10 kHz. Although the gain of the standard CPM drastically decreases with the frequency higher than approximately 60 Hz, that of the developed system has a constant gain without phase shift. The voltage of the plate is maintained with the charge decay time of 83 minutes. The insulation resistance estimated by the decay time according to an equation is $R = t/C$ and is 0.23 × 10^{9}Ω. The time required for decaying 5% of initial charging voltage is 243 seconds, which is satisfied for the evaluation of the performance of the corona discharge ionizer [28].

Figure 10 shows the typical waveform of the charged voltage of the developed CPM in the case of evaluating the charge decay time of an ionizer. The initial charge voltage to the plate is ±1.1 kV and is decayed exponentially by the ions generated by the ionizer. Generally, the charged decay time is defined as the time required to decay to ±0.1 kV from ±1.0 kV. When the plate voltage assumes a steady-state condition after electrostatic elimination, the average value of the plate voltage is defined as the ion balance or the offset voltage.

Figure 11 shows the equivalent circuit model of the electrostatic elimination system using a corona discharge ionizer. The ionizer and the charged object are connected by the deionizing space. The v_O is the output voltage of the high-voltage power supply applied to the electrode of electrostatic eliminator. C_A is the stray capacitance and is on the order of 10^{-12} F. R_{ion} is resistance expressed by the ion flow and is on the order of 10^8–10^{10} Ω [27]. C_{obj} and R_{obj} are the capacitance and the leakage resistance of the charged object, respectively. Since the high-voltage supply (ionizer) and the object (CPM) are coupled by C_A, the voltage synchronized to v_O is induced on C_{obj}. In the electrostatic elimination system shown in **Figure 8**, the voltage is induced on the ion-trapping plate of the CPM and is induced by the electric field emitted from the ionizer in the same manner. Additionally, the ions generated by the corona discharges flow into the plate electrode through R_{ion}. The polarity of the ion flows into the plate is the same as the phase of v_O. Therefore,
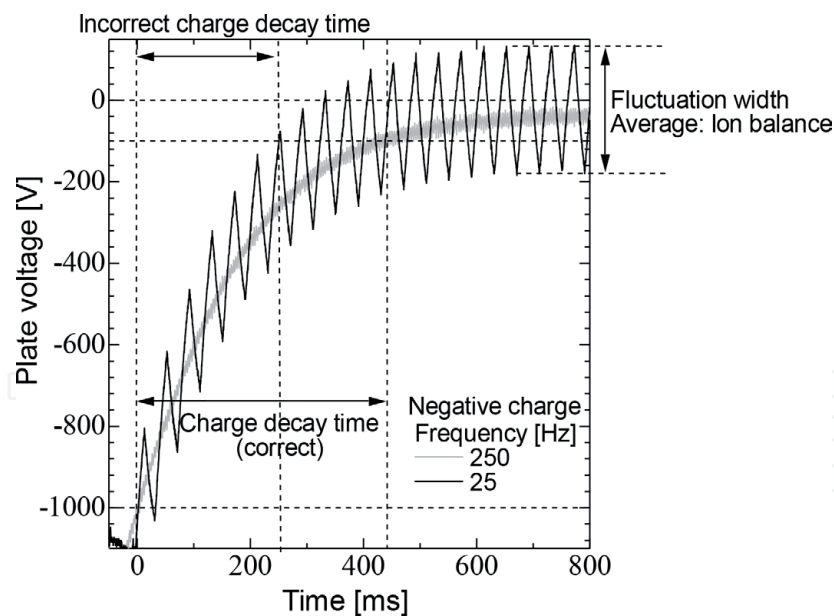
Figure 10.
Typical waveform of the plate voltage in the case of negative charged electrostatic elimination for two frequencies.
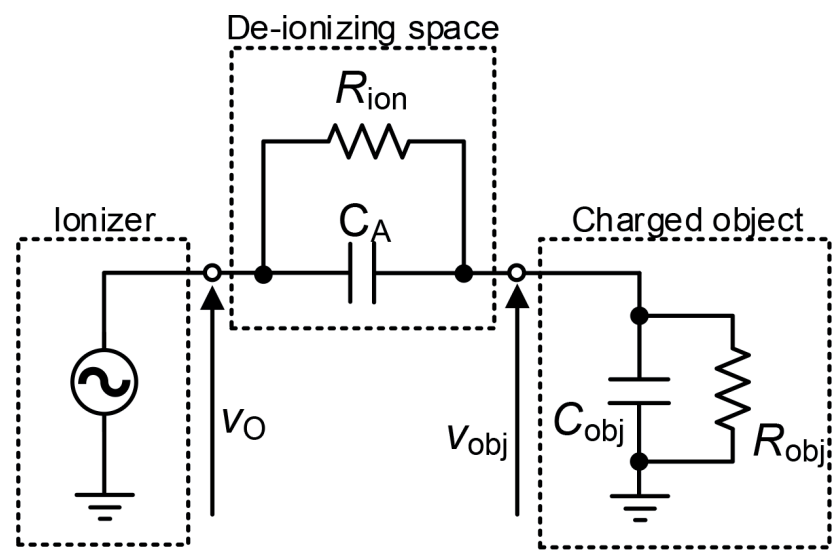

Figure 11.
Equivalent circuit model of the electrostatic elimination system using a corona discharge ionizer.

the plate voltage fluctuates during the steady-state condition after electrostatic elimination. **Figure 12** shows the example waveforms of a high voltage applied to an electrode of an electrostatic eliminator, the plate voltage, an induced voltage by high voltage, and a voltage generated by an ionic flow current to the plate. A rectangular waveform with a frequency of 1 kHz is applied to the electrostatic eliminator. The induced voltage is estimated by the electric field from the electrostatic eliminator using a probe [30]. The voltage due to the ionic current is estimated by subtracting the induced voltage from the plate voltage. The plate voltage is induced by the electric field and the ionic current, which causes a fluctuation of the voltage potential of the object.

This fluctuation is submerged when the CPM's frequency characteristics are not sufficiently high for the frequency of the voltage applied to the electrostatic eliminator, which could lead to unexpected ESD problems. Additionally, the fluctuation could lead to underestimation of the charge decay time because some CPMs define
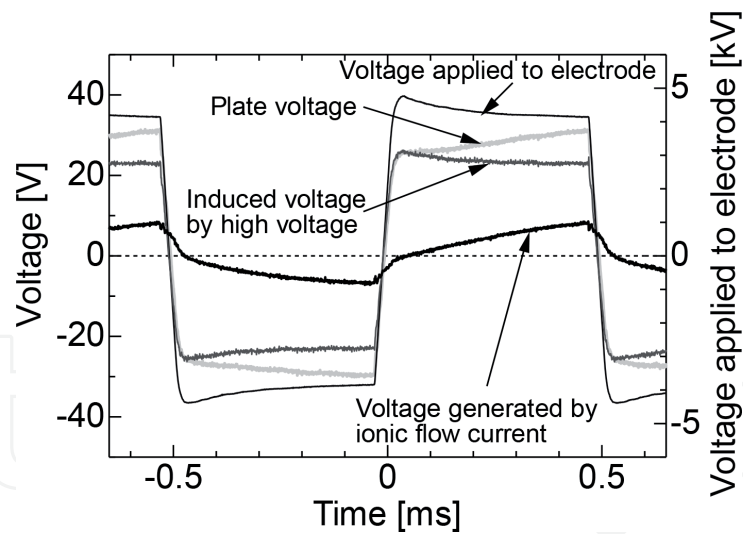
Figure 12.
Example waveforms of a high voltage applied to an electrode of an electrostatic eliminator, the plate voltage, an induced voltage by the high voltage, and a voltage generated by an ionic flow current to the plate.

the charge decay time when the plate voltage reaches to ±0.1 kV at once, although it should be measured with the time averaged voltage as shown in **Figure 8**. The precise evaluation of the voltage potential of the object is vitally important for high-level ESD control.

4. Characteristics of electrostatic elimination using bipolar pulse voltage with blown air

Figure 13 shows the charge decay time as a function of air velocity of the blown air using two intermittent bipolar pulsed voltages, uncontrolled with the ringing and controlled close to an ideal condition, as shown in **Figure 5** [26]. A bar-type corona discharge ionizer (Shishido electrostatic, CABX-350L) is used as the ionizer
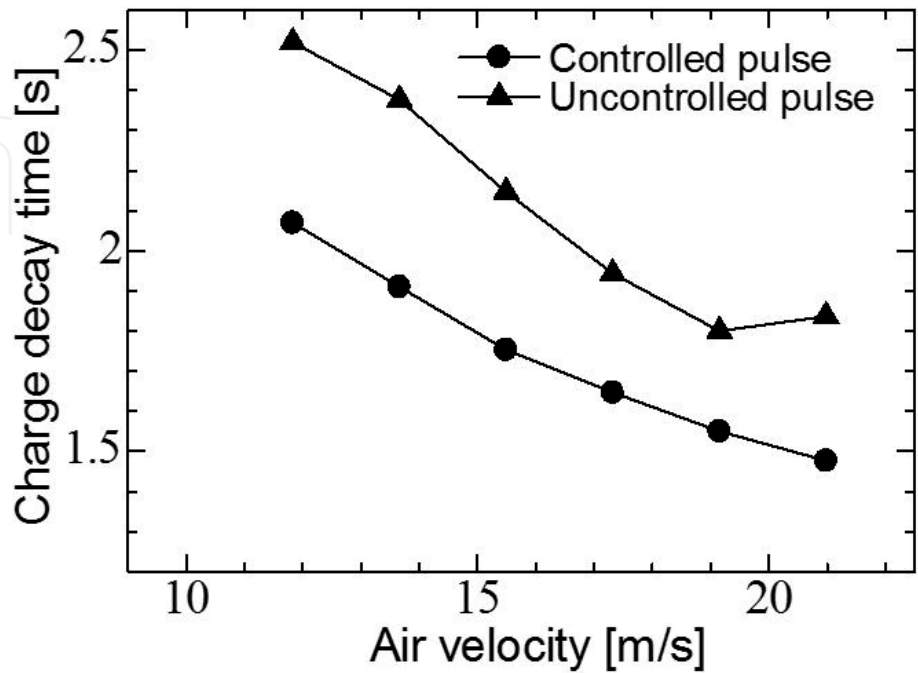

Figure 13.
Charge decay time as a function of air velocity using two intermitted bipolar pulsed voltages, controlled and uncontrolled pulses to inhibit ringing [26].
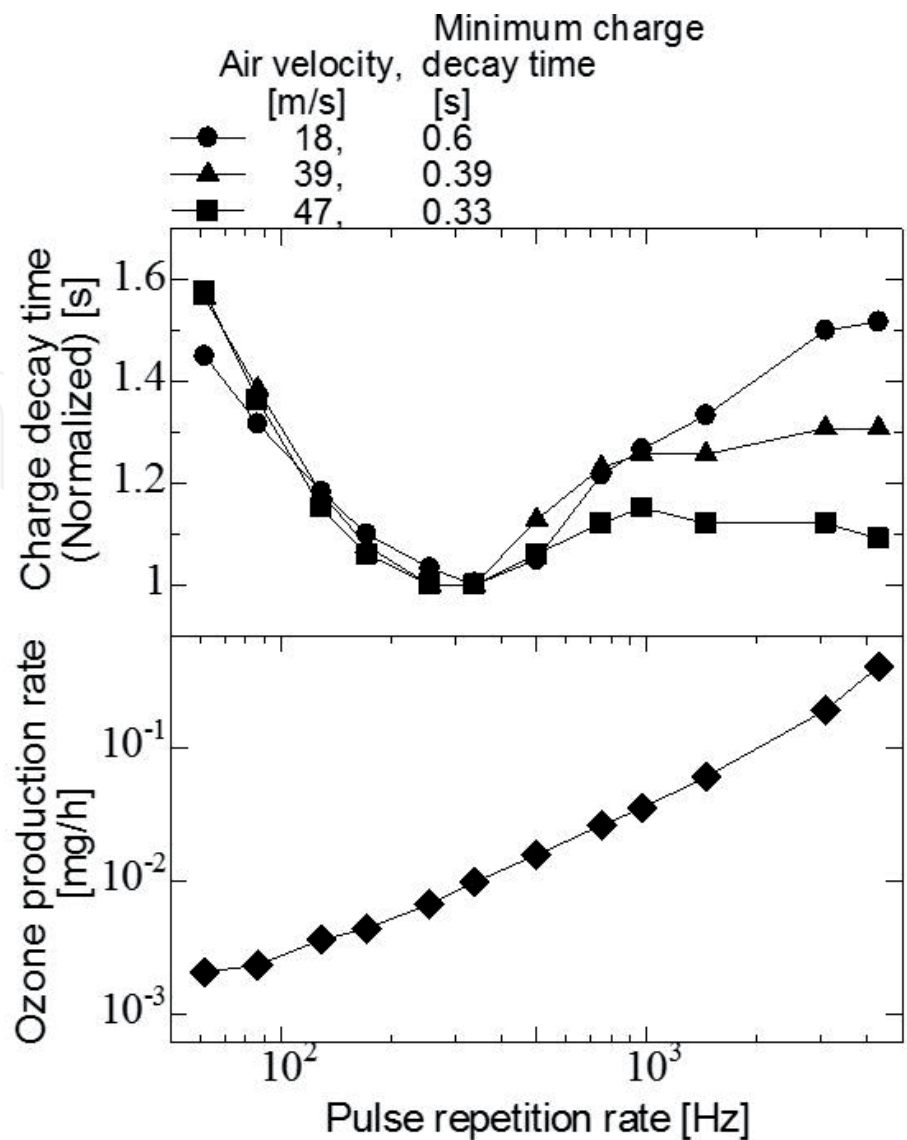
Figure 14.
Charge decay time and ozone production rate as a function of pulse repetition rate [26].

with the air blown by compressed air. The air velocity is measured at 10 mm in front of the needles. The amplitude and pulse repetition rate of the pulsed voltage are 7.5 kV and 250 Hz, respectively. The charge decay time in the case of controlled pulsed voltage is much shorter than that of uncontrolled pulsed voltage.

Figure 14 shows the charge decay time and the ozone production rate as a function of the pulse repetition rate. The pulse width is fixed at 0.2 ms. The charge decay time is normalized by the minimum charge decay time for each air velocity. The ozone concentration is determined by an ozone monitor (Ebara, EG-2001). The charge decay time has a minimum at the pulse repetition rate of 250 Hz. The ozone concentration increases with increasing pulse repetition rate. Since ozone is produced by the ionization reactions in the corona discharges, the amount of ions produced by the corona discharges increases with the ozone concentration [31]. The charge decay time depends on the ion flux into the ion-trapping plate and decreases with increasing ion concentration. The number of corona discharges per unit time decreases with decreasing pulse repetition rate, which decreases the ion concentration and increases the charge decay time. On the other hand, with increasing pulse repetition rate, the ions dragged toward the needles by Coulomb force decrease, and the amount of ions lost by the recombination reactions at the vicinity of the needle increases. Therefore, the charge decay time has a minimum value at the pulse repetition rate of 250 Hz. Because the time of flight of the ions decreases with increasing

the air velocity, the recombination reactions of ions in the deionizing space decrease. Thus, the increase in the charge decay time is suppressed with the higher air velocity, as shown in **Figure 14**. The uncontrolled pulse waveform with ringing, as shown in **Figure 5**, has a higher-frequency component than the controlled pulse waveform. This is one of the reasons that the charge decay time in the case of an uncontrolled pulse is higher than that of a controlled pulse as shown in **Figure 13**.

The corona needle electrodes are degraded with a dust attachment to the electrode, a crystallization of a neutral gas molecule, such as siloxane, at the tip of the electrode, and an erosion of the electrode by an etching effect of corona discharge [32–35]. The performance of the electrostatic eliminator is degraded with needle degradation, which leads to an increase in the charge decay time due to the decrease in ion production and the collapse of the ion balance with unbalanced ion production. The increase in the ions that do not contribute to the electrostatic elimination, such as ions lost by recombination reactions, causes the degradation of the needle electrode, which is strongly affected by the frequency and the waveform of the applied voltage to the electrode. The optimization of frequency and waveform is important for improving the efficiency of electrostatic elimination and maintaining performance during long-term operation.

The ion balance can be controlled by the timing of pulse generation. **Figure 15** shows the ion balance as a function of the pulse duty ratio. The pulse duty ratio, a timing of pulse generation, is defined as shown in **Figure 5b**. The ion balance linearly increases with increasing pulse duty ratio with a controlled pulse, which enables the easy control of ion balance. Generally, the ion balance has been controlled with the amplitude of the voltages in the cases of DC and AC type ionizers. **Figure 16** shows the time change of the plate voltage using three different types of high-voltage power supply: DC, a commercialized frequency (50 Hz), and an intermittent pulse (250 Hz). The amplitude of the voltage is fixed at 7 kV in every type of high-voltage power supply. The fluctuation of the plate voltage is suppressed using the intermittent pulse type in comparison with the others because the corona discharge and ion production are stable. The ion balance control by the duty ratio of the intermittent pulse enables an easy and rapid control of the ion balance, which also contributes to long-term stability.
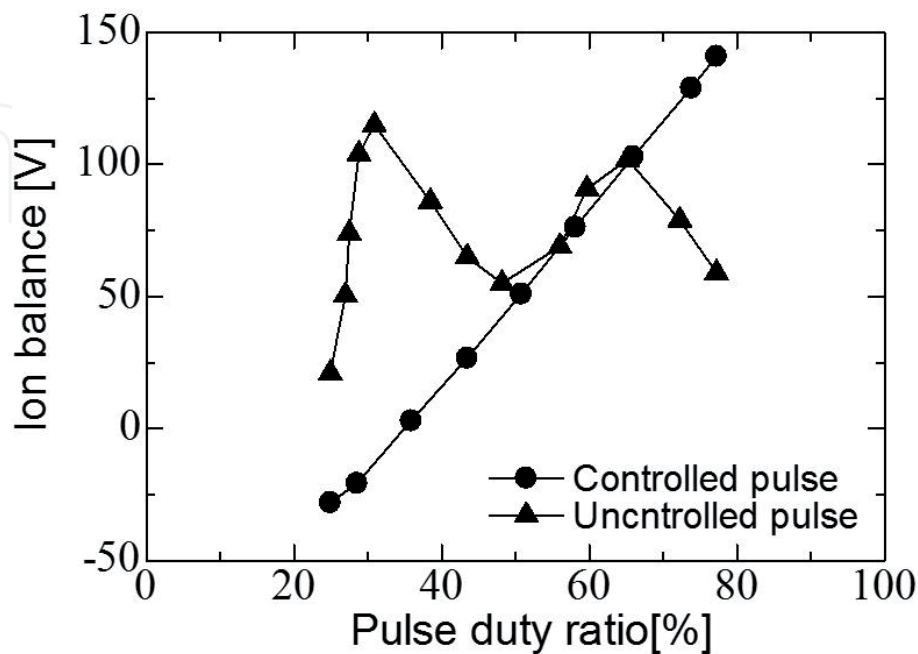

Figure 15.
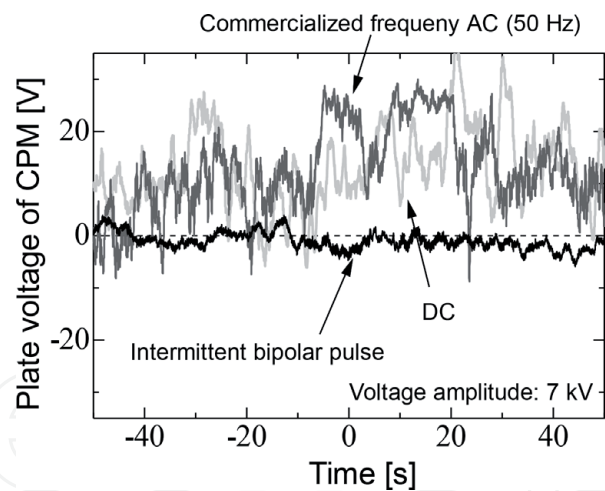*Ion balance as a function of pulse duty ratio [26].*

Figure 16.
Time change of the plate voltage using three different types of high-voltage power supply.
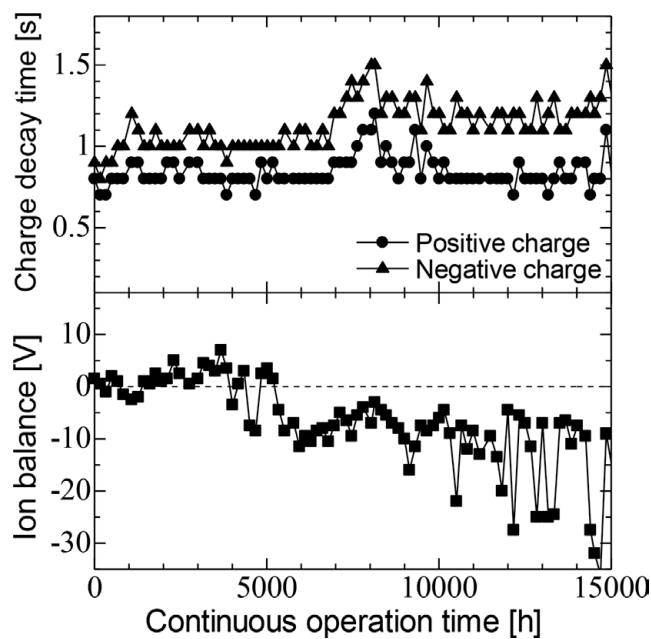
Figure 17.
Time change of the charge decay time and ion balance of a corona discharge electrostatic eliminator driven by the bipolar intermittent pulse voltage.

Figure 17 shows the time change of the charge decay time and the ion balance of a corona discharge electrostatic eliminator driven by the bipolar intermittent pulse voltage. The performance is maintained for 15,000 hours, several times longer than conventional commercial frequency AC and DC types. Recently, a perfectly balanced fan-type ionizer utilizing an intermittent pulse AC voltage power supply has been developed [36]. The short-term fluctuation range of the offset voltage is smaller than ±2 V without a sensor feedback system, which has maintained 2500 hours of continuous operation. The charge decay times are also maintained. The electric field expanded from this electrostatic eliminator has an insignificant effect on the voltage potential of the object. This ionizer is very promising for electrostatic elimination situations requiring an extremely low-offset voltage (ion balance), such as a magnetic head slider used in hard disc drives where the ion balance is restricted to a maximum of 2–10 V in the manufacturing process [15, 16, 17].

5. Electrostatic elimination without blown air

Generally, the ions produced by the corona discharges are transported to the electrostatic charged objects by blown air using a fan or a compressed air. The charge decay time decreases with increasing the air velocity as shown in **Figure 13** and is mainly dominated by the air velocity [13, 37–41]. However, blown air is limited in many situations, such as the electrostatic elimination of light weight objects and those in a clean room. In these situations, the ions are mainly transported to the objects by the Coulomb force with the electric field between the electrodes and the objects. In the cases of AC and bipolar pulse voltages, the ions are not efficiently accelerated with the rapid polarization change, which causes the decrease of the electrostatic elimination efficiency due to the increase of ion recombination loss. Therefore, a low-frequency voltage waveform is suitable for electrostatic elimination without blown air. However, as mentioned above, in a high-voltage power supply using a transformer, the magnetic flux inside the core required to magnetically couple the primary and secondary windings increases with decreasing frequency, which increases in the size and weight of the transformer. To generate a low-frequency voltage with a small and lightweight transformer, the same polarity pulse train is continuously generated in a phase by the PWM converter, as shown in **Figure 6**. **Figure 18** shows the typical waveforms of the applied voltage and the plate voltage of the CPM using the continuously generated pulses. The plate voltage continuously increases in the phase in which the same polarity pulses are continuously generated. The results show that the ions flowing into the plate and the phase have the same polarity.

When the same polarity current flows to the primary side of the transformer, the magnetic core is magnetically saturated, which decreases the amplitude and pulse width of the output voltage and causes ringing. To prevent magnetic saturation, a counter pulse with a low voltage is generated before the main pulse voltage. **Figure 19** shows the typical waveforms of pulse voltage with and without the counter pulses and the bipolar intermittent pulse. The counter pulse prevents magnetic saturation, which inhibits ringing after the main pulse and decreases the amplitude and pulse width of the pulse voltage. **Figure 20** shows the charge decay time with and without the counter pulses. Without blown air, the electrostatic charge is efficiently eliminated by the continuously generated pulses. The charge decay time
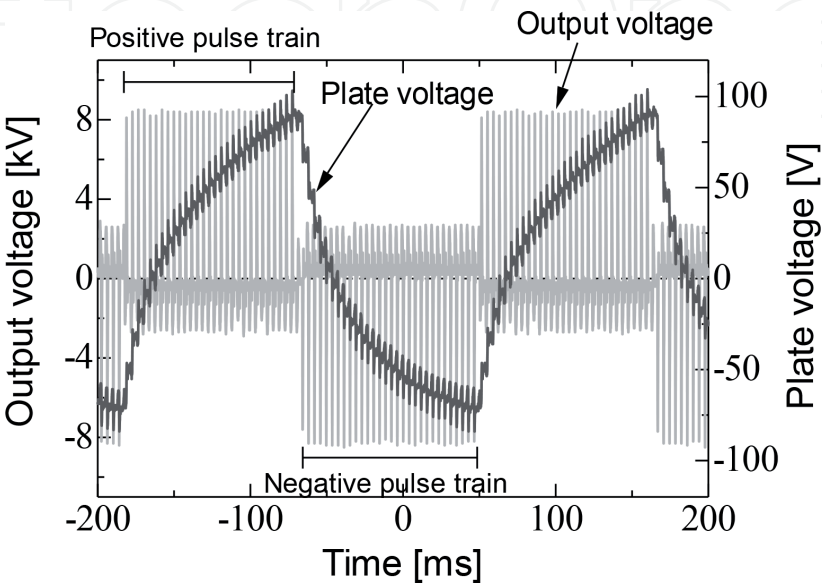

Figure 18.
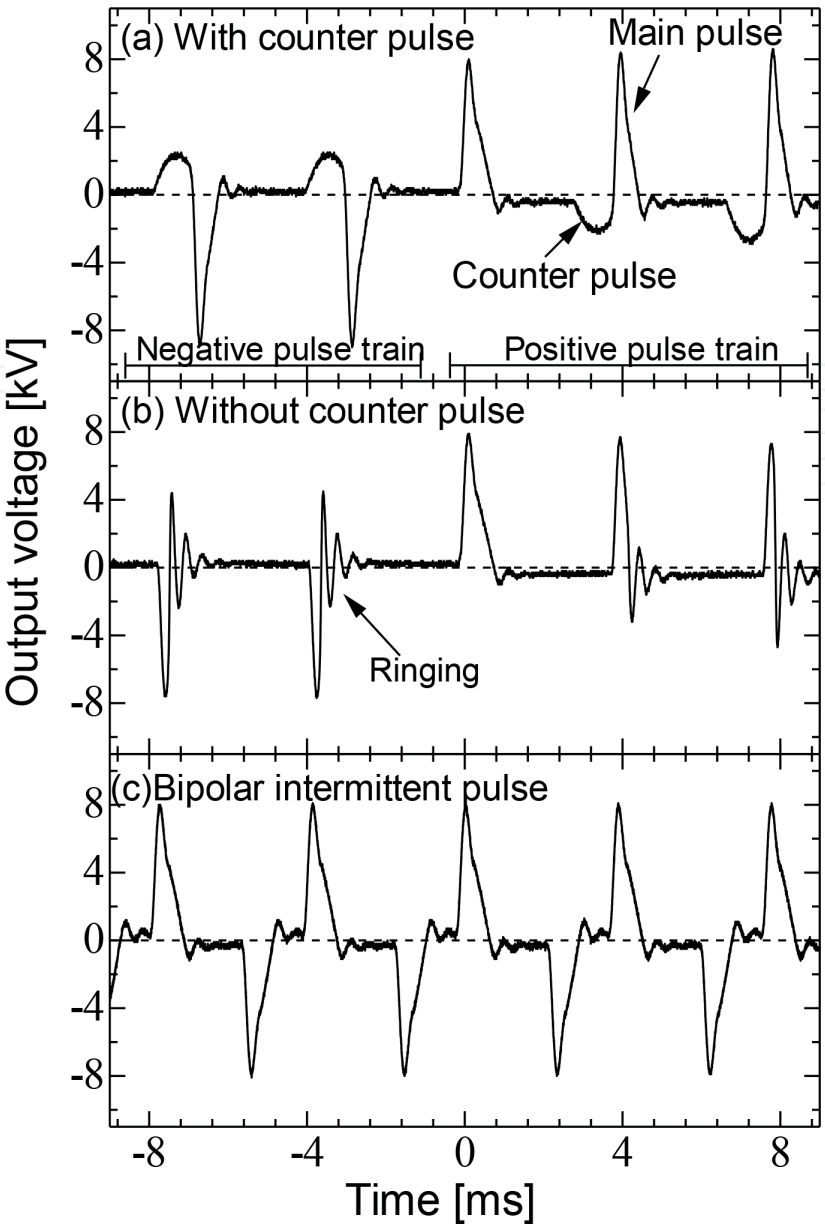*Typical waveforms of the applied voltage and the plate voltage of CPM.*

Figure 19.
Typical waveforms of pulse voltage with and without the counter pulses and the bipolar intermittent pulse [26].
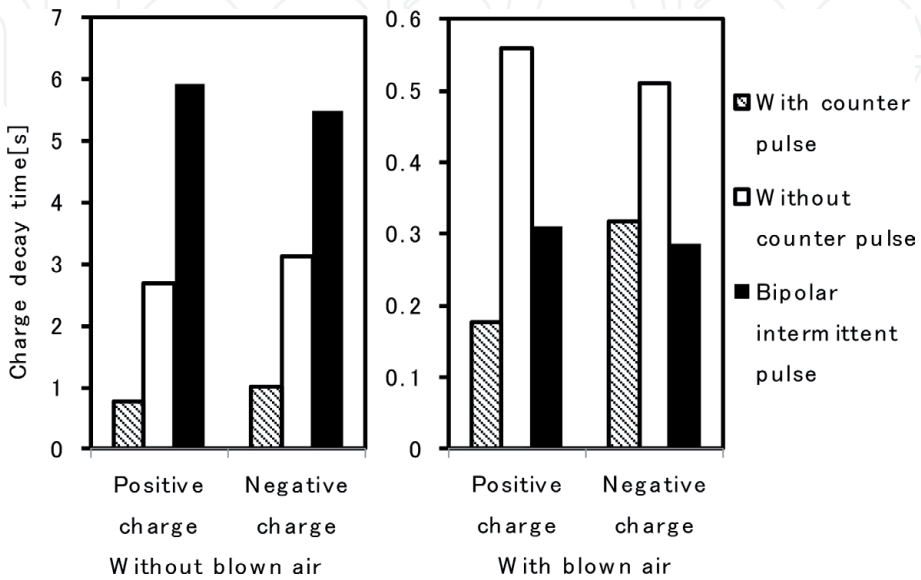

Figure 20.
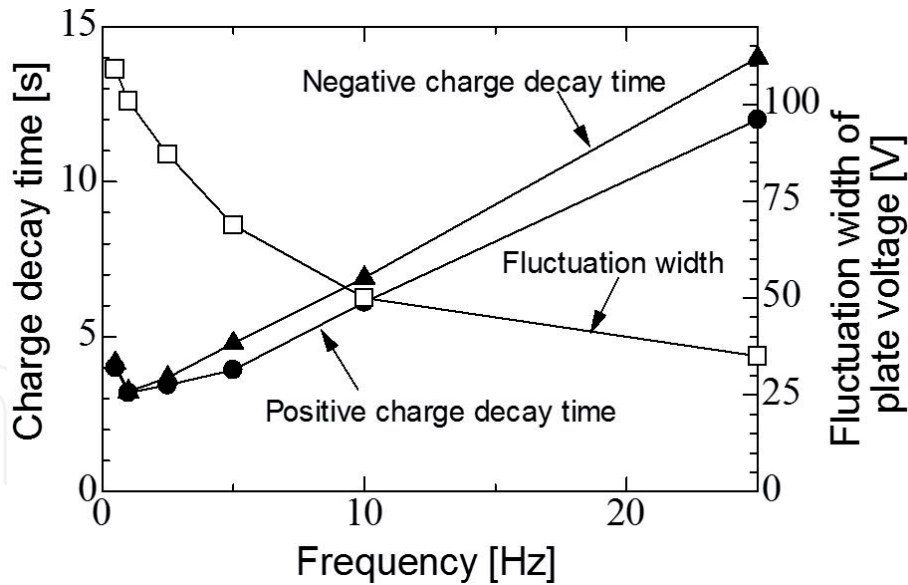*Charge decay time with and without the counter pulses [26].*

Figure 21.
Charge decay time and the fluctuation width of the plate voltage as a function of the frequency of the voltage phase [26].

with the counter pulses is shorter than that without the counter pulses. In the case of the bipolar intermittent pulse, the charge decay time is over six times longer than that of the continuously generated pulses. The ozone concentration produced by the corona discharges in the case of this method is 0.011 mg-O_3/h and is lower than that with a conventional commercial frequency AC voltage, at 0.017 mg-O_3/h. The results show that the efficiency of electrostatic elimination is much higher than conventional methods. With blown air **Figure 20b**, the charge decay time with the counter pulse is shorter than that without the counter pulses. The decrease of the amplitude and pulse width decreases the ion production and the efficiency of ion transportation as shown in **Figure 20a**.

As shown in **Figures 12** and **18**, the same polarity ions as the applied voltage continuously flow into the plate at the same polarity phase, and the plate voltage increases according to the polarity. **Figure 21** shows the charge decay time and the fluctuation width of the plate voltage as a function of the frequency of the voltage phase. The fluctuation width is measured during the steady-state condition as shown in **Figure 10**. The charge decay time and the fluctuation width increase with decreasing frequency. Without blown air, the lower frequency is suitable for the electrostatic elimination; however, it causes a large fluctuation of the voltage potential on the objects. When the capacitance and the limitation of the voltage potential of the objects are low, suppressing the fluctuation of the voltage potential is required. The developed method can generate pulse voltages with wide-range frequencies ranging from several Hz to several kHz using the same transformer and circuit, which can adjust to various situations.

6. Conclusion

An intermittent pulse voltage AC power supply controlled by a PWM inverter with a small and lightweight transformer has been developed for highly efficient electrostatic elimination, and its specifications as an electrostatic eliminator have been highlighted. The PWM control can provide a flexible control of the frequency, pulse width, and amplitude of the voltage waveform applied to the corona discharge electrode. A certain degree of freedom in generating the pulse voltages and the waveforms can be optimized in various applications, which enables the design

of small and lightweight systems. The charge decay time, the time required to eliminate electrostatic charge on a charged object, is evaluated using the charge plate monitor with a high-frequency characteristic for accurate measurements. The efficiency for electrostatic elimination increases with increasing velocity of blow air and has a maximum value with pulse repetition rate of around 250 Hz in the case of intermittent bipolar pulse voltages. The high-efficiency electrostatic elimination can be realized with the optimization of the waveforms, which contributes to a long-term performance stability. The intermittent pulse voltage AC power supply can contribute to the various processes such as the processes which require very good ion balance.

Conflict of interest

The authors declare no conflict of interest.

Author details

Katsuyuki Takahashi[1,2*], Koichi Takaki[1,2], Isao Hiyoshi[3], Yosuke Enomoto[3], Shinichi Yamaguchi[1,3] and Hidemi Nagata[3]

1 Faculty of Science and Engineering, Iwate University, Morioka, Iwate, Japan

2 Agri-Innovation Center, Iwate University, Morioka Iwate, Japan

3 Shishido Electrostatic, Ltd., Yokohama, Japan

*Address all correspondence to: ktaka@iwate-u.ac.jp

IntechOpen

References

[1] Greason WD, Castle GSP. The effects of electrostatic discharge on microelectronic devices a review. IEEE Transactions on Industry Applications. 1984;**IA-20**:247-252. DOI: 10.1109/TIA.1984.4504404

[2] Lerner A. A new additive for electrostatic discharge control in foams and elastomers. Journal of Cellular Plastics. 1985;**21**:31. DOI: 10.1177/0021955X8502100103

[3] Vinson JE, Liou JJ. Electrostatic discharge in semiconductor devices: An overview. Proceedings of the IEEE. 1998;**86**:399-418. DOI: 10.1109/5.659493

[4] Vinson JE, Liou JJ. Electrostatic discharge in semiconductor devices: Protection techniques. Proceedings of the IEEE. 2000;**88**:1878-1900. DOI: 10.1109/ICMEL.2000.840579

[5] Greason WD, Castle GSP. Review of the effect of electrostatic discharge and protection techniques for electronic systems. IEEE Transactions on Industry Applications. 1987;**IA-23**:205-216. DOI: 10.1109/TIA.1987.4504895

[6] Nagato K, Matsui Y, Miyata T, Yamauchi T. An analysis of the evolution of negative ions produced by a corona ionizer in air. International Journal of Mass Spectrometry. 2006;**248**:142-147. DOI: 10.1016/j.ijms.2005.12.001

[7] Nagato K, Nakauchi M. Experimental study of particle formation by ion-ion recombination. The Journal of Chemical Physics. 2014;**141**:164309. DOI: 10.1063/1.4898376

[8] Inaba H, Ohmi T, Morita M, Nakamura M. Neutralization of wafer charging in nitrogen gas. IEEE Transactions on Semiconductor Manufacturing. 1992;**5**:359-367. DOI: 10.1109/66.175368

[9] Inaba H, Sakata S, Yoshida T, Okada T, Ohmi T. Antistatic protection in wafer drying process by spin-drying. IEEE Transactions on Semiconductor Manufacturing. 1992;**5**:234-240. DOI: 10.1109/66.149814

[10] Manninen HE, Franchin A, Schobesberger S, Hirsikko A, Hakala J, Skromulis A, et al. Characterisation of corona-generated ions used in a neutral cluster and air ion spectrometer (NAIS). Atmospheric Measurement Techniques. 2011;**4**:2767-2776. DOI: 10.5194/amt-4-2767-2011

[11] Kraz V. Notes on maintaining Sub-1V balance of an ionizer. In: Proceedings of the 2004 Electrical Overstress/Electrostatic Discharge Symposium; 19-23 September 2004; Grapevine, TX, USA; pp. 1-6. DOI: 10.1109/EOSESD.2004.5272608

[12] Levit L, Wallash A. Measurement of the effects of ionizer imbalance and proximity to ground in MR head handling. Journal of Electrostatics. 1999;**47**:375-382. DOI: 10.1016/S0304-3886(99)00040-6

[13] Chang JS. Neutralization theory of static surface charges by an ionizer under wide gas pressure environments. IEEE Transactions on Industry Applications. 2012;**37**:1641-1645. DOI: 10.1109/28.968172

[14] Takahashi K, Sato M, Ohkubo T, Fujiwara T, Takaki K. 2-D measurement of charged particles diffusing from a double DC corona discharge ionizer. IEEE Transactions on Plasma Science. 2013;**41**:1863-1868. DOI: 10.1109/TPS.2013.2252610

[15] Mizoh Y, Nakano T, Tagashira K, Nakamura K, Suzuki T. Soft ESD phenomena in GMR heads in the HDD manufacturing process. Journal of Electrostatics. 2006;**64**:72-79. DOI: 10.1016/j.elstat.2005.03.090

[16] Wallash A, Smith D. Electromagnetic interference (EMI) damage to giant magnetoresistive (GMR) recording heads. In: Proceedings of Electrical Overstress/ Electrostatic Discharge Symposium; 6-8 October 1998; Reno, NV, USA; pp. 368-374. DOI: 10.1109/ EOSESD.1998.737058

[17] Baril L, Nichols M, Wallash A. Degradation of GMR and TMR recording heads using very-short-duration ESD transients. IEEE Transactions on Magnetics. 2002;**38**:2283-2285. DOI: 10.1109/ TMAG.2002.802803

[18] Paasi J. Assessment of ESD threats to electronic components. Journal of Electrostatics. 2005;**63**:589-596. DOI: 10.1016/j.elstat.2005.03.021

[19] Asano K, Fukada Y, Yasukawa T. Measurement of AC ion current from a corona ionizer using a Faraday cage. Journal of Electrostatics. 2008;**66**:275-282. DOI: 10.1016/j.elstat.2008.01.006

[20] Ohsawa A, Nomura N. Continuously balanced pulse-DC ioniser to minimise the offset voltage. Journal of Electrostatics. 2016;**79**:16-19. DOI: 10.1016/j.elstat.2015.11.005

[21] Jones JE, Davies M, Goldman A, Goldman B. A simple analytic alternative to Warburgs law. Journal of Physics D: Applied Physics. 1990;**23**:542-552. DOI: 10.1088/0022-3727/23/5/012

[22] Ohsawa A. Modeling of charge neutralization by ionizer. Journal of Electrostatics. 2005;**63**:767-773. DOI: 10.1016/j.elstat.2005.03.043

[23] Ohsawa A. Computational comparison of charge neutralisations of conductors and insulators with corona ionisers. Journal of Electrostatics. 2004;**62**:219-230. DOI: 10.1016/j. elstat.2004.05.009

[24] Dordizadeh P, Adamiak K, Castle GSP. Experimental study of the characteristics of Trichel pulses in the needle-plane negative corona discharge in atmospheric air. Journal of Electrostatics. 2017;**88**:49-54. DOI: 10.1016/j.elstat.2016.12.013

[25] Frylladitakis ED, Moronis AX, Theodoridis MP. A mathematical model for determining an electrohydrodynamic accelerator's monopolar flow limit during positive corona discharge. IEEE Transactions on Plasma Science. 2017;**45**:432-440. DOI: 10.1109/TPS.2017.2663778

[26] Takahashi K, Hiyoshi I, Enomoto Y, Nagata H. Development of an electrostatic eliminator utilizing high voltage AC power supply driven by PWM inverter. Journal of International Electrostatics Japan. 2014;**38**:124-129

[27] Takahashi K, Goto A, Nagata H. Development of an electrostatic eliminator utilizing compact high-voltage AC power supply. Journal of International Electrostatics Japan. 2015;**39**:238-241

[28] ANSI/ESD STM3.1-2015. ESD association standard test method for the protection of electrostatic discharge susceptible items—Ionization: ESD Association; 2015

[29] Crowley JM, Leri D, Dahlhoff G, Levit L. Equivalent circuits for air ionizers used in static control. Journal of Electrostatics. 2004;**61**:71-83. DOI: 10.1016/j.elstat.2003.11.006

[30] Takahashi K, Kaga H, Kubo K, Takaki K, Yamaguchi S, Nagata H. Development of an ion measuring system for AC corona discharge. IEEJ Transactions on Fundamentals and Materials. 2018;**138**:551-552. DOI: 10.1541/ieejfms.138.551

[31] Chen J, Davidson JH. Electron density and energy distributions in the

positive DC corona: Interpretation for corona-enhanced chemical reactions. Plasma Chemistry and Plasma Processing. 2002;**22**(2):199-224. DOI: 10.1023/A:1014851908545

[32] Chen J, Davidson JH. Ozone production in the negative DC corona: The dependence of discharge polarity. Plasma Chemistry and Plasma Processing. 2003;**23**:501-518. DOI: 10.1023/A:1023235032455

[33] Noll CG, Lawless PA. Comparison of germanium and silicon needles as emitter electrodes for air ionizers. Journal of Electrostatics. 1998;**44**:221-238. DOI: 10.1016/ S0304-3886(98)00015-1

[34] Petrov AA, Amirov RH, Samoylov IS. On the nature of copper cathode erosion in negative corona discharge. IEEE Transactions on Plasma Science. 2009;**37**:1146-1149. DOI: 10.1109/TPS.2009.2018561

[35] Weissler GL. Positive and negative point-to-plane corona in pure and impure hydrogen, nitrogen and argon. Physical Review. 1943;**63**:96-107. DOI: 10.1103/PhysRev.63.96

[36] Takahashi K, Goto A, Yamaguchi S, Saito T, Sakamoto K, Nagata H. Development of a perfectly balanced electrostatic eliminator utilizing an intermittent pulse AC voltage power supply. In: Proceedings of 2015 37th Electrical Overstress/ Electrostatic Discharge Symposium (EOS/ESD), 27 September-2 October 2015; Reno, NV, USA; DOI: 10.1109/ EOSESD.2015.7314753

[37] Ohsawa A. Efficient charge neutralization with an ac corona ionizer. Journal of Electrostatics. 2007;**65**:598-606. DOI: 10.1016/j.elstat.2007.01.003

[38] Osawa A. 2-D electrohydrodynamic simulations towards zero offset voltage with corona ionisers. Journal of Electrostatics. 2013;**71**:116-124. DOI: 10.1016/j.elstat.2012.12.021

[39] Noll C. Charge-carrier extraction from air and nitrogen gas streams that entrain charge from DC corona ionizers. Journal of Electrostatics. 2002;**54**:271-282. DOI: 10.1016/ S0304-3886(01)00170-X

[40] Intra P, Tippayawong N. Design and evaluation of a high concentration high penetration unipolar corona ionizer for electrostatic discharge and aerosol charging. Journal of Electrical Engineering and Technology. 2013;**8**:1175-1181. DOI: 10.5370/ JEET.2013.8.5.1175

[41] Intra P, Tippayawong N. Effect of needle cone angle and air flow rate on electrostatic discharge characteristics of a corona-needle ionizer. Journal of Electrostatics. 2010;**68**:254-260. DOI: 10.1016/j.elstat.2010.01.008